Optimizing Cr(VI) and Tc(VII) remediation through nano-scale biomineral engineering

Richard S. Cutting[1], Victoria S. Coker [1], Neil D. Telling[1,3], Richard L. Kimber[1], Carolyn I. Pearce[1], Beverly Ellis[2], Richard Lawson[2], Gerrit van der Laan [3,1], Richard A.D. Pattrick[1], David J. Vaughan[1], Elke Arenholz[4] and Jonathan R. Lloyd[1]*

[1]Williamson Research Centre for Molecular Environmental Science, and School of Earth, Atmospheric and Environmental Sciences, University of Manchester, Manchester M13 9PL, UK

[2]Department of Nuclear Medicine, Manchester Royal Infirmary, Oxford Road, Manchester, M13 9WL, UK

[3]Magnetic Spectroscopy Group, Diamond Light Source, Didcot, Oxfordshire, OX11 0DE, UK

[4]Advanced Light Source, Lawrence Berkeley National Laboratory, Berkeley, CA, USA

*richard.cutting@manchester.ac.uk

Keywords: chromium**,** technetium, bioreduction, ferrihydrite, schwertmannite, *Geobacter sulfurreducens*, biogenic magnetite, remediation

Abstract

To optimise the production of biomagnetite for the bioremediation of metal oxyanion contaminated waters, the reduction of aqueous Cr(VI) to Cr(III) by two biogenic magnetites and a synthetic magnetite was evaluated under batch and continuous flow conditions. Results indicate that nano-scale biogenic magnetite produced by incubating synthetic schwertmannite powder in cell suspensions of *Geobacter sulfurreducens* is more efficient at reducing Cr(VI) than either biogenic nano-magnetite produced from a suspension of ferrihydrite "gel" or synthetic nano-scale Fe_3O_4 powder. Although X-ray Photoelectron Spectroscopy (XPS) measurements obtained from post-exposure magnetite samples reveal that both Cr(III) and Cr(VI) are associated with nanoparticle surfaces, X-ray Magnetic Circular Dichroism (XMCD) studies indicate that some Cr(III) has replaced octahedrally coordinated Fe in the lattice of the magnetite. Inductively Coupled Plasma-Atomic Emission Spectrometry (ICP-AES) measurements of total aqueous Cr in the associated solution phase indicated that, although the majority of Cr(III) was incorporated within or adsorbed to the magnetite samples, a proportion (~10-15 %) was released back into solution. Studies of Tc(VII) uptake by magnetites produced via the different synthesis routes also revealed significant differences between them as regards effectiveness for remediation. In addition, column studies using a γ-camera to obtain real time images of a ^{99m}Tc(VII) radiotracer were performed to visualise directly the relative performances of the magnetite sorbents against ultra-trace concentrations of

metal oxyanion contaminants. Again, the magnetite produced from schwertmannite proved capable of retaining more (~20 %) ^{99m}Tc(VII) than the magnetite produced from ferrihydrite, confirming that biomagnetite production for efficient environmental remediation can be fine-tuned through careful selection of the initial Fe(III) mineral substrate supplied to Fe(III)-reducing bacteria.

Introduction

Chromium contamination of soils, sediments and ground waters is a world-wide problem arising as a result of the use of the metal in a range of industrial processes, including leather tanning, pulp production, wood treatment, electroplating and various other metallurgical applications *(1)*. Natural sources of chromium include the weathering of serpentinised ultramafic rocks leading to the formation of soils that locally may contain levels of Cr in excess of 80,500 mg kg^{-1} *(2-4)*. In the natural environment, chromium may participate in numerous oxidation-reduction reactions that can dramatically alter its chemical properties. Typically, Cr occurs in two stable oxidation states, Cr(III) and Cr(VI), which exhibit very different toxicological and transport characteristics *(3,5)*. Hexavalent chromium is a strong oxidising agent known to be toxic to plants *(6)*, animals *(7,8)* and humans *(9)*. In mammals, Cr(VI) is tetratogenic *(10)*, mutagenic *(11)* and carcinogenic *(9,12)*. The dangers posed by the toxicity of Cr(VI) are increased by its occurrence as an oxyanion that is only weakly adsorbed by mineral surfaces *(4)*, and the fact that it does not form a stable (oxyhydr)oxide. As a consequence, Cr(VI) is highly mobile *(2,13)*. In contrast, Cr(III) can be regarded as effectively immobile in most environments due to the low solubility of Cr(III)-(oxyhydr)oxides, and the formation of strong sorption complexes at the surfaces of soil minerals *(3)*. The relatively low toxicity of Cr(III) is due primarily to these factors, coupled with poor biological uptake and adsorption *(14,15)*.

The World Health Organization (WHO) has set a maximum acceptable guideline concentration of 0.5 mg l^{-1} for chromate in drinking water *(16)*. In many instances,

compliance with this guideline requires the treatment of industrial effluents prior to discharge into municipal waste water systems *(5)*. Existing chemical and electrochemical treatment strategies involve reducing aqueous Cr(VI) to Cr(III), accompanied by pH adjustment in order to precipitate the Cr(III) ions *(5)*. There are also a number of Cr(VI) treatment strategies that utilise chemical reductants to form Cr(III) *(5)*. These involve the use of low solubility Fe(II)-bearing compounds such as magnetite *(17)*, or Fe electrodes *(18-20)*, or reduced sulfur-bearing compounds *(3,5)*.

The aim of the present work is to compare both the rate and efficiency of Cr(VI) reduction by synthetic and biogenic nanoparticulate magnetites produced by the Fe(III)-reducing bacterium *Geobacter sulfurreducens*, under both batch and continuous flow conditions. The atomic-scale mechanism of Cr(VI) reduction/immobilization at the magnetite-solution interface has been investigated by measurements of Cr and Fe in solution and studies of the solids and surfaces using X-ray diffraction (XRD), X-ray photoelectron spectroscopy (XPS), transmission electron microscopy (TEM) and X-ray magnetic circular dichroism (XMCD) before and after exposure to aqueous Cr(VI). The impact of dissolved oxygen on Cr(VI) reduction has also been investigated. Cr(VI) reduction by the synthetic and biomagnetites in columns was also monitored, and these experiments were augmented by experiments in which a γ-camera was used to visualise directly the migration of a ^{99m}Tc(VII) (TcO_4^-) radiotracer. This approach also allowed the total radioactivity associated with the influent and effluent flows to be measured directly, and confirmed the enhanced performance of biologically synthesized magnetite in remediation of systems containing ultra-trace concentrations of toxic metal oxyanions.

Experimental

Magnetite formation

A ferrihydrite "gel" was produced by forced alkaline hydrolysis of a $FeCl_3.6H_2O$ solution (*Sigma Aldrich*) as described by *(21)*, the resulting precipitate was stored as a suspension at 4°C in 18.2 MΩ water. Schwertmannite was prepared using a modified version of the method described by *(22)*. The precipitate was washed six-times in 18.2 MΩ water, freeze dried and stored under a nitrogen atmosphere until required.

An isolate of *G. sulfurreducens* was obtained from our laboratory culture collection and grown under anaerobic conditions at 30°C in modified fresh water medium *(23)*. Sodium acetate (20 mM) and fumarate (40 mM) were provided as the electron donor and acceptor, respectively. All manipulations were performed under an atmosphere of N_2-CO_2 (80:20). Late log-phase cultures of *G. sulfurreducens* were harvested by centrifugation (4920 *g* for 20 minutes) and washed twice in bicarbonate buffer ($NaHCO_3$; 30 mM, pH 7.1) under N_2-CO_2 (80:20) gas. Aliquots of the washed cell suspension (0.3ml) were added to sealed anaerobic bottles containing bicarbonate buffer and 0.1 g or ~ 0.5 ml of the appropriate Fe(III)-bearing starting material. The final concentration of bacteria was 0.6 mg protein per ml. Additions of sodium acetate (20 mM) and AQDS (10 μM) were made from anaerobic stocks as required to give a total volume of 10ml. Bottles were incubated at 20°C in the absence of light. Analyses were carried out to determine the 0.5 M and 3 M HCl-extractable Fe(II) using the ferrozine method *(21)*. Following incubation, biogenic magnetites were concentrated

using a magnet and washed twice in anaerobic deionised water under anoxic conditions. The resulting solids were then resuspended in 10 ml of anaerobic water and stored in sealed glass serum bottles, prior to use in Cr(VI) and ^{99m}Tc(VII) reduction studies.

Analytical techniques

XRD measurements were performed using a *Bruker* instrument (*D8Advance*), with a Cu $K_{\alpha 1}$ source. The instrument was equipped with a Göbel mirror and all data were obtained using Soller slits on both the X-ray tube and the detector, the antiscatter slits were wide open (3^{o}). Diffraction data was acquired over a range of 15° 2θ – 70° 2θ, with a step size of 0.02° 2θ.

TEM images and Selected Area Electron Diffraction (SAED) patterns were acquired using a *Phillips/FEI CM200*, equipped with a Field Emission Gun, EDX system (*Oxford Instruments UTW ISIS*) and a Gatan Imaging Filter and with an operating beam voltage of 200keV. A droplet of each of the dispersions was placed on holey carbon grids (*Agar*) and allowed to dry prior to imaging.

XPS data were recorded using a *Kratos* instrument (*Axis Ultra*) employing a monochromated Al K_{α} X-ray source and an analyser pass energy of 20 eV, resulting in a total energy resolution of ca. 0.9 eV. The system base pressure was 5×10^{-10} mbar. Samples were loaded into the spectrometer via a dry nitrogen glove box to avoid exposure to atmospheric oxygen. Photoelectron Binding Energies (BE) were referenced to C 1*s* adventitious contamination peaks set at 285 eV BE. The analyser was calibrated using

elemental references: Au $4f_{7/2}$ (83.98 eV BE), Ag $3d_{5/2}$ (368.26 eV BE) and Cu $2p_{3/2}$ (932.67 eV BE). Fitting of XPS data involved subtraction of an appropriate background from all spectra *(24)*. Synthetic components (70% Lorentzian: 30% Gaussian) were then assigned to the Fe 2*p* region based on multiplet splitting calculations performed for free Fe ions *(25,26)*.

X-ray adsorption spectra (XAS) spectra were obtained on station 4.0.2 at the Advanced Light Source (Berkeley, CA, USA), using an octopole magnet end station *(27)*. Samples of magnetite were analysed both before and after exposure to Cr(VI), to assess the effect on the oxidation state and site occupancy of both Fe and Cr. XAS were monitored in Total-Electron Yield (TEY) mode, which gives an effective probing depth of ~4.5 nm. At each energy point the XAS were measured for the two opposite magnetization directions by reversing the 0.6 Tesla applied field. The spectra for the two magnetization directions were normalised to the incident beam intensity and subtracted to give the XMCD spectrum *(28)*. The measured Fe $L_{2,3}$ XMCD was used to obtain the site occupancies of the Fe cations in the spinel structure of biogenic magnetite precipitates, see *(29-31)* for details.

Batch chromate reduction experiments

Batch Cr(VI) reduction experiments involved known amounts of magnetite slurry and a solution of Cr(VI) (potassium chromate) at a Cr(VI) concentration of either 0.1 mM, 0.5 mM, 1 mM or 5 mM in a total volume of 10 ml. All bottles, other than those used to investigate the influence of dissolved oxygen, had a head-space comprising N_2(g), with 1.2 % H_2(g). For aerobic systems, bottles were exposed to atmospheric oxygen prior

to experimentation in order to allow equilibration. All bottles were stored at 20 °C in the dark

Chromate and pertechnetate column reduction experiments

Continuous flow experiments were performed in glass columns measuring 300 mm in length and 30 mm in diameter. A cotton wool bung was placed at the bottom of the column, followed by a 3 cm layer of high purity natural quartz (Congleton) sand *(32)*. This was followed by a layer of ferrihydrite derived magnetite, as a slurry of known concentration with a volume of either 1.08 ml, 2.16 ml, 5.4 ml, 25 ml or 125 ml and covered with an additional layer of Congleton sand. An aqueous solution containing Cr(VI) (50 μmol) was pumped through the column using a peristaltic pump (*Watson Marlow 205S*); the flow direction was from the bottom of the column to the top. The solution pumping rate was fixed at 15 ml h^{-1}, resulting in an average residence time of approximately 5 h in the column. Effluent samples (5 ml) were removed from the top of the column for determination of aqueous Cr(VI). All experiments, unless otherwise stated, were conducted at room temperature under anaerobic conditions and with light excluded from the influent Cr(VI) solution. A column that contained only Congleton sand was used as a control.

Additional column studies aimed at reducing Tc(VII) (TcO_4^-) to Tc(IV), analogous to the Cr(VI) reduction experiments, were conducted at Manchester Royal Infirmary using ultra-trace concentrations of ^{99m}Tc. A gamma-camera (*GE3 Low Energy High Resolution*) was used to directly visualise the activity of ^{99m}Tc present within the

column system. The influent solution was spiked with 10 ml of Tc(VII) stock solution, and followed by deionised water. The total activities of the influent ^{99m}Tc solutions were determined to be 20 MBq, 24.1 MBq and 21.7 MBq for the control, ferrihydrite-derived magnetite and schwertmannite-derived magnetite-bearing columns respectively. The columns were placed in front of the gamma camera and the influent solutions were pumped through the systems, and the effluent solutions were collected in a separate vessel, sequential images were acquired for 5 min at regular 20 min intervals for the first hour, and then at 30 minute intervals up to 14 h. Any activity remaining in the effluent containers was also measured using the gamma camera. Columns without magnetite were used as controls throughout. Somewhere you need to mention the approx molar conc of the Tc.

Iron and chromium analyses

Following the incubation of both ferrihydrite and schwertmannite with *G. sulfurreducens*, several serum bottles containing the post-reduction minerals were sacrificed in order to accurately determine total Fe concentration. Following digestion in conc? hydrofluoric acid (HF) the concentration of Fe present within each serum bottle was determined using Inductively Coupled Plasma Atomic Emission Spectrometry (ICP-AES) (*Perkin- Elmer, Optima 5300DV*).

Batch Cr(VI) reduction experiments were sampled regularly, and aliquots of slurry were removed in order to determine total Fe and total Cr remaining in solution. These samples were filtered to remove any particulate material prior to dilution and

acidification using 2 % HNO_3 (*Analar, BDH*). All samples were then stored in the dark at 4˚ C prior to analysis by ICP-AES. Columns were sampled by removing a 5 ml aliquot from the effluent at the top of the column at predetermined times. The Cr(VI) concentration in all experiments was determined using the DPC spectrophotometric assay *(33)*.

Results and Discussion

Characterization of starting materials and biogenic solids

Both the starting materials (ferrihydrite "gel" and schwertmannite powder) and the resulting biogenic magnetites were characterised using X-ray Diffraction (XRD). Details of these analyses have been published previously *(34,35)*. These studies indicate that, for both starting materials, extended incubation with *G. sulfurreducens* results in the conversion of a poorly ordered Fe(III)-containing material to a highly crystalline biogenic magnetite.

TEM images and Selected Area Electron Diffraction (SAED) patterns for both starting materials indicate that the ferrihydrite gel, when dried, is a fine grained material with a particle size of ~2 nm [Figure 1(a)]. By contrast, images of the schwertmannite sample reveal a chaotic mixture of randomly orientated polycrystalline whiskers that are ~30-40 nm in length and less than ~5 nm in width similar to the synthetic schwertmannite described by *(36)* (Figure 1(b)). TEM images of the samples after extended incubation with *G. sulfurreducens* are consistent with a change in mineralogy to a highly crystalline material. The appearance of lattice fringes and the corresponding SAED pattern indicate

that the biotransformation product is magnetite. Both samples are shown to have a roughly spherical particle morphology with an approximate particle size of 10-20 nm [Figure 1(c) and (d)].

High-resolution Fe 2*p* XPS data obtained from ferrihydrite and schwertmannite show that Fe $2p_{3/2}$ peaks occur at ~711.3 eV and 711.6 eV BE respectively, characteristic of ferric iron *(25)*,*(35)*. Changes in the solid state Fe speciation during incubation with *G. sulfurreducens* are highlighted by Fe 2*p* XPS obtained from synthetic magnetite, ferrihydrite-derived magnetite and schwertmannite-derived magnetite (see Figure 2) where two satellites are present at ~716 eV BE and ~719 eV BE that are characteristic of mixed valence Fe minerals such as magnetite (Fe_3O_4).

Kinetics of Cr(VI) reduction by magnetite

Batch reduction experiments were performed with fixed initial Cr(VI) concentrations of 0.1 mM, 0.5 mM, 1 mM or 5 mM. For experiments with Cr(VI) concentrations of either 0.1 mM or 0.5 mM, both biogenic magnetites were able to rapidly remove all of the Cr(VI) from solution. For an initial Cr(VI) concentration of 1 mM both biogenic magnetites were able to remove significantly more aqueous Cr(VI) than synthetic magnetite (Figure 3). After 300 min incubation, synthetic magnetite was able to remove 58 % (C/C_0 = 0.42) of the Cr(VI), whilst ferrihydrite-derived magnetite and schwertmannite-derived magnetite were able to remove 70% (C/C_0 = 0.3) and 95% (C/C_0 = 0.05) of the total Cr(VI), respectively.

When the concentration of Cr(VI) was increased to 5 mM, f-magnetite and s-magnetite were able to reduce 0.92 mM ($C/C_0 = 0.82$) and 1.7 mM ($C/C_0 = 0.66$) of the total Cr(VI) respectively. In keeping with experiments performed at lower initial Cr(VI) concentrations, the biogenic schwertmannite-derived magnetite sample was able to reduce 85 % more Cr(VI) than ferrihydrite-derived magnetite. This will be addressed in more detail below in terms of an electron balance for the two half reactions $Cr(VI) + 3e^- \leftrightarrow Cr(III)$ and $3Fe^{2+} - 3e^- \leftrightarrow 3Fe^{3+}$.

Effect of oxygen fugacity

The activity of dissolved oxygen is a key factor affecting systems in which aqueous Cr(VI) reduction is coupled to the oxidation of Fe(II). Data obtained following the exposure of ferrihydrite-derived magnetite and schwertmannite-derived magnetite to 0.1 mM and 0.5 mM Cr(VI), under either anaerobic or aerobic conditions, are shown in Figure 4. Under anaerobic conditions, complete removal of Cr(VI) from a 0.1 mM solution was achieved within 40 minutes using biogenic magnetite synthesised from either starting material (Figure 4). Similar rapid removal of Cr(VI) occurred under anaerobic conditions when either biogenic magnetite was added to a 0.5 mM Cr(VI) solution, with all Cr(VI) removed after 430 minutes (Figure 4). However, under aerobic conditions although s-magnetite completely removed all Cr(VI) from a 0.5 mM solution in only 430 minutes, f-magnetite only removed 46% of the 0.5 mM Cr(VI) solution over the same time period (Figure 4).

The precise reasons for the observed differences in susceptibility of the magnetite samples to oxygen exposure are not fully understood. However, XPS results shown in our previous studies *(35)* and in Figure 2(iii) indicate that the near-surface region of schwertmannite-derived magnetite is reduced with respect to stoichiometric Fe_3O_4. The Fe(II):Fe(III) ratio of the schwertmannite-derived magnetite is 58:42 based on fitting of XPS data. By contrast, the Fe(II):Fe(III) ratio for ferrihydrite-derived magnetite is 24:76 [Figure 2(ii)]; thus, ferrihydrite-derived magnetite contains 35 % less Fe(II) at or near the surface than schwertmannite-derived magnetite. Iron speciation data obtained using ferrozine assay following total digestion in 3 M HCl indicate that the bulk schwertmannite-derived magnetite contains 17 % more Fe(II) than ferrihydrite-derived magnetite. Comparison of this bulk Fe(II) measurement with the surface sensitive (approximately 60 Å maximum analysis depth) XPS data indicates that the near surface regions of schwertmannite-derived magnetite crystallites are enriched in Fe(II) by ~ 18 % relative to the bulk. We directly attribute differences in aqueous Cr(VI) reduction between the two biogenic samples to the relatively high concentration of Fe(II) in the near-surface region of schwertmannite-derived magnetite. Furthermore, we propose that for s-magnetite, the excess Fe(II) associated with the surface region exists as sorbed Fe^{2+}, possibly serving to stabilize the over-reduced Fe_3O_4-solution interface when in contact with an oxidizing aqueous solution. Numerous authors have demonstrated the heightened performance of particulate mineral suspensions when prepared with adsorbed Fe^{2+} in various reduction experiments *(37-44)*.

Electron balance and reaction stoichiometry

For a stoichiometric redox reaction, 3 mol of Fe(II) are required in order to reduce 1 mol of Cr(VI) to Cr(III). However, previous authors have demonstrated that for aqueous Fe(II), between 3 and 4 equivalents were required in order to reduce 1 equivalent of Cr(VI), and that the reaction product is a mixed iron(III)-chromium(III) hydroxide at neutral pH *(5,45)*. In the present study, the Cr(VI) reduction efficiency has been determined in two different ways. Firstly, results are expressed based on the assumption that all of the magnetite samples are stoichiometric Fe_3O_4 and that 3 mol of Fe(II) are required to reduce 1 mol of Cr(VI). Too eliminate systematic bias, all Cr(VI) reduction data presented here are normalised to total Fe concentration. Therefore, either enrichment or depletion of Fe(II) relative to stoichiometric Fe_3O_4 will result in an increase or decrease in Cr(VI) reduction capacity. For systems containing ferrihydrite-derived magnetite, the total Fe concentration was 131.2 mM i.e. equivalent to a magnetite concentration of 44 mM or 10.1 g l^{-1}. For schwertmannite-derived magnetite, the total Fe concentration was 83.0 mM i.e. equivalent to a magnetite concentration of 27.7 mM or 6.4 g l^{-1}. If one assumes initially that both biogenic magnetites were stoichiometric Fe_3O_4, then suspensions of ferrihydrite- and schwertmannite-derived magnetite contained the equivalent of 14.6 mM and 9.2 mM Fe(II), respectively. Thus, assuming the participation of structural Fe(II), the maximum amount of Cr(VI) that should have been reduced by the ferrihydrite-derived magnetite suspension is equivalent to 4.86 mM, whilst s-magnetite should have been capable of reducing 3.1 mM Cr(VI), assuming 100 % efficiency. Experiments were performed where initial Cr(VI) concentrations in the contacting solutions were 0.1 mM (5.2 mg l^{-1}), 0.5 mM (26 mg l^{-1}), 1 mM (104 mg l^{-1}) or 5 mM (260 mg l^{-1}). As mentioned above, a batch with an initial Cr(VI) concentration of 5 mM

yielded C/C_0 values of 0.66 for s-magnetite and 0.82 for ferrihydrite derived magnetite. Hence, schwertmannite-derived magnetite was able to reduce 21 % more Cr(VI) than the maximum expected for stoichiometric Fe_3O_4; by contrast, ferrihydrite-derived magnetite reduced 48 % less. As mentioned above, XPS results indicated the near-surface region of s-magnetite contains 35 % more Fe(II) than ferrihydrite-derived magnetite, whereas bulk digests indicate that the average Fe(II) enrichment is only 17 %. Furthermore, XPS analysis of ferrihydrite-derived magnetite yielded an Fe(II):Fe(III) ratio of 24:76, indicating that the near surface region was slightly oxidized with respect to stoichiometric Fe_3O_4. Thus, if the Cr(VI) data are normalised to total surface Fe(II), ferrihydrite-derived magnetite should have been capable of completely reducing at the most, a 1.7 mM solution of Cr(VI). The decrease in Cr concentration of 0.92 mM reported here suggests that ~81 % of the total Fe(II) present within ferrihydrite-derived magnetite was unavailable for Cr(VI) reduction. By contrast, schwertmannite-derived magnetite should have been capable of reducing, at most, between 3.6 mM and 4.1 mM of Cr(VI) compared with 1.7 mM of Cr(VI) actually reduced. Thus, for the schwertmannite-derived biogenic magnetite, between 41 % and 47 % of the total Fe(II) remained following equilibration with a 5 mM Cr(VI) solution. The discussion above clearly suggests that the redox reaction between aqueous Cr(VI) and Fe(II) present at the surface of s-magnetite involves Fe(II) ions located within the bulk of particles, and is not restricted entirely to ions located immediately at the mineral-solution interface. This point will be further discussed below.

Characterization of biogenic magnetites following exposure to Cr(VI)

TEM images of biogenic magnetite samples after exposure to a 5 mM Cr(VI) solution are shown in Figure 1(e-f). Inspection of these images, particularly at particle margins did not reveal the presence of a second phase . Particles remained well crystalline with a size of 10-20 nm, although they appeared to become more rounded in shape with a more unifoem particle size distribution.. We interpret these changes as the result of particle ripening in response to exposure to aqueous chromate. Similar changes in iron oxide nanoparticle morphology due to interfacial redox reactions have been documented *(46)*.

Following exposure to a 5 mM aqueous Cr(VI) solution, XPS data obtained from all three magnetites revealed the presence of Cr [Figure 5(b)]. Fitting of the main Cr 2*p* peaks indicated that each comprise two components at 576.7 eV and 578.3 eV and 586.7 eV and 588.6 eV BE for schwertmannite-derived magnetite and 576.8 eV and 578.6 eV and 586.7 eV and 588.4 eV BE for ferrihydrite-derived magnetite [see Figure 5(b)(ii-iii)]. A review of previous studies *(1,47-49)*, together with our own XPS analyses of a range of pure Cr salts, indicates that for Cr(VI), the $2p_{3/2}$ peak is located between 579 eV-579.8 eV BE, and that spin–orbit splitting observed for Cr(VI) is 8.7 eV-9.4 eV *(1,47,48)*. By contrast, for Cr(III) the $2p_{3/2}$ component occurs between 576.5 eV-576.9 eV BE and the spin-orbit splitting associated with Cr(III) is 9.9 eV *(1,47,48)*. Thus, we clearly see a mixture of Cr(III) and Cr(VI) at the surfaces of the magnetite samples [Figure 5(b)(i-iii)].

Corresponding high-resolution Fe 2*p* XPS data obtained from the same samples as the Cr 2*p* spectra are presented in Figure 5(a). All spectra exhibit a decrease in the

intensity of the low-binding energy shoulder associated with the Fe $2p_{3/2}$ feature, located at ~709 eV BE (cf. Figure 2). This change, coupled with an increase in the intensity of the satellite feature located at ~719 eV BE, indicates that the near-surface regions of all the magnetite samples tested here had been oxidised in response to exposure to aqueous Cr(VI), in agreement with the Cr 2*p* XPS results that indicate some of the Cr(VI) had been reduced to Cr(III), most likely by the Fe(II) associated with the magnetite.

In order to investigate the mechanism of Cr(VI) reduction by magnetite, additional measurements were made on the same magnetite samples using XMCD. For the Fe $L_{2,3}$-edge, the intensities of the three peaks labelled A, B and C in Figure 6(a) correspond to the site occupancies of the Fe^{2+} O_h, Fe^{3+} T_d and Fe^{3+} O_h, respectively (for further details, see *(29)*). XMCD spectra for f-magnetite and s-magnetite before and after exposure to a 5 mM Cr(VI) solution show a consistent trend with a decrease in Fe(II) corresponding to an increase in Fe(III) on O_h sites as shown by the cation site occupancy data in Figure 6(a). Figure 6(b) shows the Cr $L_{2,3}$-edge adsorption and XMCD spectra for both magnetites following exposure to 5 mM Cr(VI); these are similar to the reference spectrum of the antiferromagnetic mineral Cr_2O_3 *(50)*. However, since our samples display a distinct XMCD signal [Figure 6(b)], which is impossible for an antiferromagnetic material, the Cr is likely to be in the 3+ oxidation state but in a material which is ferrimagnetic. In fact, the data are most similar to Cr(III) in a spinel-structured compound, as our line-shapes are almost identical to *(51)* ($CrFe_2O_4$) and similar to *(50)* (Cr-thiospinels), where $CrFe_2O_4$ is a normal spinel in which the Cr(III) resides in the octahedral (O_h) sites, whilst Fe(II) occupies tetrahedral (T_d) sites *(51)*. Based on the

similarity of the calculated XAS and XMCD data to those obtained for $CrFe_2O_4$ *(30)*, we conclude that the Cr(III) is situated, at least partially, within the spinel lattice of the magnetite, and located on O_h sites. Examination of the Fe $L_{2,3}$–edge offers support to this model as, from the calculated fits in Figure 6(a), the amount of Fe(III) gained is not completely accounted for by the loss of Fe(II), as would be expected if magnetite oxidation was the only process occurring. The difference is most likely due to the incorporation of Cr(III) and suggests the formation of a Cr-spinel layer in both biogenic magnetite samples. However, from the ratios of the XAS peak heights of Cr and Fe for each sample, the schwertmannite magnetite sample contains approximately twice as much Cr as the ferrihydrite-derived magnetite. The large difference in total Cr can be accounted for by examination of the Cr $L_{2,3}$-edge XMCD spectra [Figure 6(b)], as for schwertmannite-derived magnetite, the relative size of the XMCD spectrum is weaker (and noisier) than that obtained for ferrihydrite-derived magnetite. An explanation for a decrease in the magnetic signal in schwertmannite-derived magnetite, despite the presence of more total Cr, could be the presence of a capping layer of material containing non-magnetic Cr above the Cr-spinel layer on the schwertmannite-derived magnetite; this would contribute to the XAS spectrum, but not the XMCD spectrum. This suggests that schwertmannite-derived magnetite is able to adsorb a greater amount of a Cr(III) and Cr(VI) within this non-magnetic surface layer compared to ferrihydrite-derived magnetite. This interpretation does not preclude the possibility that ferrihydrite-derived magnetite also has a Cr oxyhydroxide layer, but it must be a thinner layer than that associated with schwertmannite-derived magnetite.

Our data suggest that the atomic-scale structure of the evolving magnetite-solution interface differs somewhat from models presented by previous authors *(1,49)*. From a mechanistic point of view, our Cr(VI) reduction kinetic data indicate that the uptake and reduction of CrO_4^{2-} ions occurs rapidly at magnetite surfaces. Following uptake, Cr(VI) is reduced to Cr(III) as a result of the transfer of electrons from three Fe^{2+} ions located at or near the magnetite surface. Comparison of Cr(VI) reduction data obtained using the DPC spectrophotometric assay, total aqueous Cr measurements made using ICP-AES and XPS Cr 2*p* data obtained following exposure to Cr(VI) show that, although a proportion of the Cr (~14 %-20 %) is retained as Cr(III) following reduction, the remainder is either adsorbed or released back into solution. This process may serve to explain the relatively high reductive capacity of biogenic magnetite, since "desorption" events may lead to "unblocking" of sites associated with Cr(VI) reduction. As mentioned above, XMCD data indicate that the retained Cr(III) is both incorporated into the spinel lattice, replacing Fe ions at O_h sites, and to some extent sorbed to the surface of the magnetite as a second, non-magnetic, phase.

Cr(VI) and ^{99m}Tc(VII) column studies

The efficiency of Cr(VI) reduction and retention by both ferrihydrite-derived magnetite and schwertmannite-derived magnetite acting as permeable reactive barriers was investigated in continuous flow column experiments containing 25 ml (approximately 250 mg) magnetite. Figure 7 shows that columns containing biogenic magnetite performed significantly better in terms of Cr(VI) retention compared to control

columns containing only Congleton sand. The concentration of Cr(VI) at the top of the control columns reached ~49 μM by 17 h after the introduction of a 50 μM Cr(VI) solution into the columns. By contrast, the concentration of Cr(VI) in columns containing either ferrihydrite-derived or schwertmannite-derived magnetite at 17 h were 14.9 μM and 11.3 μM, respectively. The concentration of Cr(VI) in the effluent solution from the control columns remained constant and approximately equal to the influent concentration throughout the experiment. However, concentrations of Cr(VI) within the effluent flow increased as a function of time within columns containing either ferrihydrite-derived or schwertmannite-derived magnetite, with maximum Cr(VI) concentrations of 45.8 μM and 27.5 μM, respectively, after 160 h. The calculated column residence time was 15 h, indicating that the Congleton sand itself can weakly attenuate Cr(VI) migration, albeit to a very limited degree in comparison to columns containing biogenic magnetite. For biogenic magnetite-bearing columns, systems containing schwertmannite-derived magnetite were able to reduce and retain ~67 % more Cr(VI) than identical columns containing ferrihydrite-derived magnetite. This result is consistent with the results of batch Cr(VI) reduction studies presented above.

In order to assess the performance of the differently synthesised magnetite minerals against trace concentrations of the redox active fission product Tc(VII), and to visualise directly the transport dynamics of the continuous flow column systems, experiments were conducted using a gamma camera and a ^{99m}Tc radiotracer (conc and activity needed here). Table 1 summarises the results of output from the imaging software that quantifies the activity detected by the gamma camera. For all column systems, the

total activity of technetium was obtained by summation of data obtained from different components present within a given system. This confirmed that no ^{99m}Tc was lost from any of the columns due to leakage. Real time and space images of the column systems containing only Congleton sand, and with either ferrihydrite-derived magnetite, or schwertmannite-derived magnetite obtained at t = 14 h, are shown in Figure 8(a).. Comparison of data presented in Table 1 and Figure 8(a) indicates that the majority of ^{99m}Tc(VII) was reduced and retained, presumably as insoluble Tc(IV) *(53)*, by the biogenic magnetite layers [Figure 8(b)]. By contrast, the control column containing only Congleton sand was almost entirely devoid of activity. For the control column, the majority (97 %) of the activity associated with the ^{99m}Tc tracer is present within the effluent solution. This result is consistent with Cr(VI) reduction studies performed in identical columns indicating that the Congleton sand, on its own, is ineffective at reducing and retaining ^{99m}Tc(VII).

Accurate scintillation counting of the effluent solutions at t = 38 h confirmed the efficiency of ^{99m}Tc retention by each column; these values are summarised in Table 2. The control column proved to be the least effective at retaining ^{99m}Tc(VII), the effluent solution contained only 16.2 % less Tc(VII) than the influent solution. Again, in agreement with Cr(VI) reduction studies, columns containing ferrihydrite-derived magnetite and schwertmannite-derived magnetite performed significantly better, retaining 77.9 % and 97.8 % respectively of the influent Tc(VII) present within the solutions, presumably via Fe(II)-mediated reduction to insoluble Tc(IV).

Our results indicate that nano-scale biogenic magnetites offer enhanced performance for the remediation of toxic anions such as Cr(VI) and Tc(VII) when compared to inorganic equivalents. Our data also suggest that the biomaterials can be tailored to some extent to suit a desired application through selection of the optimal starting Fe(III) mineral for bioreduction to magnetite. For example, magnetite derived from ferrihydrite could be preferred if the absolute amount of Cr(VI) reduced per unit mass of magnetite was not the primary concern. This material has been shown to form particles that have a magnetite centre with a Cr-ferrite rim where the Cr should be relatively resistant to remobilisation. Such materials may be particularly useful for technological or biomedical applications, given the unique magnetite properties of magnetite. On the other hand, if large scale removal and reduction of Cr(VI) is the desired goal, then schwertmannite-derived magnetite has a far greater capacity for reducing toxic Cr(VI) to the more benign Cr(III); although in this instance the thickness of the Cr-ferrite rims are reduced and a comparatively thick capping layer of non-magnetic adsorbed Cr(III) and Cr(VI) is formed. In both instance, any Cr(III) that is not either incorporated or adsorbed to magnetite particles is ultimately released back into solution. The performance of these materials *in situ* and *ex situ* remediation processes is warranted, including quantifying their transport and resistance (along with the reduced insoluble toxic metals) to reoxidation and remobilisation.

Acknowledgements

The support of EPSRC and BBSRC and NERC in funding this research is gratefully acknowledged via grants EP/D058767/1 and BB/E004601/1. Special thanks are

due to Dr Paul Wincott and Ms Catherine Davies for advice and assistance with aspects of the work. Thanks also to Dr Joyce McBeth for her assistance with Tc column studies. The Advanced Light Source is supported by the Director, Office of Science, Office of Basic Energy Sciences, of the U.S. Department of Energy under Contract No. DE-AC02-05CH11231.

References

(1) Jung, Y.; Choi, J.; Lee, W. Spectroscopic investigation of magnetite surface for the reduction of hexavalent chromium. *Chemosphere* 2007, *68*, 1968-1975.

(2) McBride, M. B. *Environmental Chemistry of Soils*; Oxford University Press: New York, 1994.

(3) Wielinga, B. W.; Mizuba, M. M.; Hansel, C. M.; Fendorf, S. Iron promoted reduction of chromate by dissimilatory iron-reducing bacteria. *Environ Sci Technol* 2001, *35*, 522-527.

(4) Oze, C.; Fendorf, S.; Bird, D. K.; Coleman, R. G. Chromium geochemistry in serpentinized ultramafic rocks and serpentine soils from the Franciscan Complex of California. *American J Sci* 2004, *304*, 67-101.

(5) Eary, L. E.; Rai, D. Chromate removal from aqueous wastes by reduction with ferrous ion. *Environ Sci Technol* 1988, *22*, 972-977.

(6) Turner, M. A.; Rust, R. H. Effects of chromium on growth and mineral nutrition of soyabeans. *Soil Sci Soc Am Proc* 1971, *35*, 755-758.

(7) Iijima, S.; Shimizu, M.; Matsumoto, N. Embryotoxic and fetotoxic effects of chromium trioxide in mice. *Teratology* 1979, *20*, 152.

(8) Danielsson, B. R. G.; Hassoun, E.; Dencker, L. Embryotoxicity of chromium: Distribution in pregnant mice and effect on embryonic cells in vitro. *Arch Toxicol* 1982, *51*, 233-245.

(9) Cohen, M. D.; Kargacin, B.; Klein, C. B.; Costa, A. M. Mechanisms of chromium carcinogenicity and toxicity. *Critical Reviews in Toxicology* 1993, *23*, 255-281.

(10) Abassi, S. A.; Soni, R. Tetratogenic effects of chromium (VI) in the environment as evidenced by the impact of larvae of amphibian *Rana Tigrina*: Implications in the environmental management of chromium. *Int. J. Environ. Stud.* 1984, *23*, 131-138.

(11) Bonatti, S.; Meini, M.; Abbondandolo, A. Genetic effects of potassium dichromate. *Mutation Research* 1976, *38*, 147-150.

(12) James, B. R.; Petura, J. C.; Vitale, R. J.; Mussoline, G. R. In *Chromium in Soil: Perspectives in Chemistry, Health, and Environmental Regulation*; Proctor, D., Finley, B., Harris, M., Paustenbach, D., Rabbe, D., Eds.; Lewis Publishers: Boca Raton, 1997; pp 561-568.

(13) Fendorf, S. E. Surface reactions of chromium in soils. *Geoderma* 1995, *67*, 55-71.

(14) Sass, B. M.; Rai, D. Solubility of amorphous Chromium(III)-Iron(III) hydroxide solid solutions. *Inorg Chem* 1987, *26*, 2228-2232.

(15) Fendorf, S.; Fendorf, M.; Sparks, D. L.; Gronsky, R. Inhibitory mechanisms of Cr(III) oxidation by δ-MnO_2. *J Colloid Interface Sci* 1992, *153*, 37-54.

(16) "Health criteria and other supporting information," World Health Organisation Geneva. 1996.

(17) Anderson, N. J.; Bolto, B. A.; Pawlowski, L. A method for chrome removal from cooling tower blowdown water. *Nuclear and Chemical Waste Management* 1984, *5*, 125-129.

(18) Fuji, K. K. K. Japan. 4051-972. 1977

(19) Moring, J. M. United States of America. 4 188 272. 1980

(20) Butler, J. W. United States of America. 3 960 722. 1984

(21) Lovley, D. R.; Phillips, E. J. P. Availability of ferric iron for microbial reduction in bottom sediments of the freshwater tidal potomac river. *Appl. Environ. Microbiol.* 1986, *52*, 751-757.

(22) Schwertmann, U.; Cornell, R. M. *Iron oxides in the laboratory*; VCH Publishers Inc: New York, 1991.

(23) Lloyd, J. R.; Leang, C.; Hodges Myerson, A. L.; Coppi, M. V.; Cuifo, S.; Methe, B.; Sandler, S. J.; Lovley, D. R. Biochemical and genetic characterization of PpcA, a periplasmic *c*-type cytochrome in *Geobacter sulfurreducens*. *Biochem. J.* 2003, *369*, 153-161.

(24) Shirley, D. A. High-Resolution X-Ray Photoemission Spectrum of the Valence Bands of Gold. *Physical Review B* 1972, *5*, 4709-4714.

(25) McIntyre, N. S.; Zetaruk, D. C. X-ray photoelectron spectroscopic studies of iron oxides. *Anal Chem* 1977, *49*, 1521-1529.

(26) Gupta, R. P.; Sen, S. K. Calculation of multiplet structure of core *p* -vacancy levels. II. *Phys Rev B* 1975, *12*, 15-19.

(27) Arenholz, E.; Prestemon, S. O. Design and performance of an eight-pole resistive magnet for soft X-ray magnetic dichroism measurements. *Reviews of Scientific Instruments* 2005, *76*, 083908/083901-083908.

(28) Pattrick, R. A. D.; van der Laan, G.; Henderson, C. M. B.; Kuiper, P.; Dudzik, E.; Vaughan, D. J. Cation site occupancy in spinel ferrites studied by X-ray magnetic circular dichroism: developing a method for mineralogists. *Eur. J. Mineral.* 2002, *14*, 1095-1102.

(29) Coker, V. S.; Pearce, C. I.; Pattrick, R. A. D.; van der Laan, G.; Telling, N. D.; Charnock, J. M.; Arenholz, E.; Lloyd, J. R. Probing the site occupancies of Co, Ni and Mn substituted biogenic magnetite using XAS and XMCD. *Am. Mineral.* 2008, *93*, 1119-1132.

(30) van der Laan, G.; Thole, B. T. Strong magnetic X-ray dichroism in 2*p* absorption spectra of 3*d* transition metal ions. *Phys Rev B* 1991, *43*, 13401-13411.

(31) van der Laan, G.; Kirkman, I. W. The 2*p* absorption spectra of 3*d* transition metal compounds in tetrahedral and octahedral symmetry. *J Phys-Condens Mat* 1992, *4*, 4189-4204.

(32) Pocock, R. *The Geology of The Country Around Macclesfield, Congleton, Crewe and Middlewich (Explanation of sheet No. 110)*; Stationary Office books, 1906.

(33) Skougstad, M. W.; Fishman, M. J.; Friedman, L. C.; Erdman, D. E.; Duncan, S. S. *Method for determination of Inorganic Substances in Water and Fluvial Sediments*; US Geological Survey: Washington DC, 1979; Vol. 5.

(34) Coker, V. S.; Bell, A. M. T.; Pearce, C. I.; Pattrick, R. A. D.; van der Laan, G.; Lloyd, J. R. Time-resolved synchrotron X-ray powder diffraction study of magnetite formation by the Fe(III)-reducing bacterium, *Geobacter sulfurreducens*. *Am Mineral* 2008, *93*, 540-547.

(35) Cutting, R. S.; Coker, V. S.; Fellowes, J. W.; Lloyd, J. R.; Vaughan, D. J. Mineralogical and morphological constraints on the reduction of Fe(III) minerals by *Geobacter sulfurreducens*. *Geochim Cosmochim Ac* 2009, DOI: 10.1016/j.gca.2009.1004.1009.

(36) Loan, M.; Cowley, J. M.; Hart, R.; Parkinson, G. M. Evidence on the structure of synthetic schwertmannite. ***Am Mineral*** **2004,** ***89,*** **1735-1742.**

(37) Klausen, J.; Troeber, S. P.; Haderlein, S. B.; Schwarzenbach, R. P. Reduction of substituted nitrobenzenes by Fe(II) in aqueous mineral suspensions. ***Environ Sci Technol*** **1995,** ***29,*** **2396-2404.**

(38) Charlet, L.; Silvester, E.; Liger, E. N-compound reduction and actinide immobilization in surficial fluids by Fe(II): the surface $FeIIIOFeIIOH^{0}$ species, as major reductant. ***Chem Geol*** **1998,** ***151,*** **85-93.**

(39) Amonette, J. E.; Workman, D. J.; Kennedy, D. W.; Fruchter, J. S.; Gorby, Y. A. Dechlorination of carbon tetrachloride by Fe(II) associated with goethite. ***Environ Sci Technol*** **2000,** ***34,*** **4606-4613.**

(40) Pecher, K.; Haderlein, S. B.; Schwarzenbach, R. P. Reduction of polyhalogenated methanes by surface-bound Fe(II) in aqueous suspensions of iron oxides. ***Environ Sci Technol*** **2002,** ***36,*** **1734-1741.**

(41) Strathmann, T. J.; Stone, A. T. Mineral surface catalysis of reactions between FeII and oxime carbamate pesticides. ***Geochim Cosmochim Ac*** **2003,** ***67,*** **2775-2791.**

(42) Elsner, M.; Schwarzenbach, R. P.; Haderlein, S. B. Reactivity of Fe(II)-bearing minerals toward reductive transformation of organic contaminants. ***Environ Sci Technol*** **2004,** ***38,*** **799-807.**

(43) Klupinski, T. P.; Chin, Y.-P.; Traina, S. J. Abiotic degradation of pentachloronitrobenzene by Fe(II): Reactions on goethite and iron oxide nanoparticles. ***Environ Sci Technol*** **2004,** ***38,*** **4353-4360.**

(44) Chun, C. L.; Holzalski, R. M.; Arnold, W. A. Degradation of drinking water disinfection byproducts by synthetic goethite and magnetite. ***Environ Sci Technol*** **2005,** ***39,*** **8525-8532.**

(45) Buerge, J.; Hug, S. J. Kinetics and pH dependence of chromium(VI) reduction by iron(II). ***Environ Sci Technol*** **1997,** ***31,*** **1426-1432.**

(46) Chun, C. L.; Penn, R. L.; Arnold, W. A. Kinetic and Microscopic Studies of Reductive Transformations of Organic Contaminants on Goethite. ***Environmental Science & Technology*** **2006,** ***40,*** **3299-3304.**

(47) Asami, K.; Hashimoto, K. The X-ray photo-electron spectra of several oxides of iron and chromium. ***Corros Sci*** **1977,** ***17,*** **559-570.**

(48) McCafferty, E.; Bernett, M. K.; Murday, J. S. An XPS study of passive film formation on iron in chromate solutions. ***Corros Sci*** **1988,** ***28,*** **559-576.**

(49) Kendelewicz, T.; Liu, P.; Doyle, C. S.; Brown, G. E.; Nelson, E. J.; Chambers, S. A. X-ray absorption and photoemission study of the adsorption of aqueous Cr(VI) on single crystal hematite and magnetite surfaces. ***Surf Sci*** **1999,** ***424,*** **219-231.**

(50) Kang, J.-S.; Kim, G.; Lee, H. J.; Kim, H. S.; Kim, D. H.; Han, S. W.; Kim, S. J.; Kim, C. S.; Lee, H.; Kim, J.-Y.; Min, B. I. Synchrotron radiation spectroscopy study of $FeCr_2X_4$ (X=S and Se). ***J. Appl. Phys.*** **2008,** ***103,*** **07D717.**

(51) Mizumaki, M.; Agui, A.; Saitoh, Y.; Nakazawa, M.; Matsushita, T. XAS and MCD studies of $CrFe_2O_4$. ***Surface Review and Letters*** **2002,** ***9,*** **849-853.**

(52) Telling, N. D.; Coker, V. S.; Cutting, R. S.; Kimber, R. L.; van der Laan, G.; Pearce, C. I.; Pattrick, R. A. D.; Arenholz, E.; Lloyd, J. R. Remediation of Cr(VI) by

biogenic magnetite nanoparticles: an X-ray magnetic circular dichroism study. ***Appl Phys Letts*** **2009, submitted.**

(53) Lloyd, J.R;, Sole, V.A.; Van Praagh, C. V. G. and Lovley, D.R. Direct and Fe(II)-mediated reduction of technetium by Fe(III)-reducing bacteria. ***Applied and Environmental Microbiology*** **2000, 66, 3743-3749.**

Table Captions

Table 1. Activity detected using a gamma camera of ^{99m}Tc (added as ^{99m}Tc (VII)) to columns containing two biomagnetite phases (derived from schwertmannite and ferrihydrite) and a synthetic magnetite control .

Table 2. Results of scintillation counting of the influent and effluent of the column systems exposed to ^{99m}Tc(VII).

Figure captions

Figure 1 Transmission electron microscopy of (a) ferrihydrite, (b) schwertmannite, (c) ferrihydrite derived magnetite (f-magnetite), (d) schwertmannite derived magnetite (s-magnetite, (e) f-magnetite exposed to 5 mM Cr(VI) solution and (f) s-magnetite exposed to 5 mM Cr(VI) solution.

Figure 2. XPS Fe 2*p* data of magnetic materials. (i) synthetic magnetite; (ii) biogenic magnetite derived from ferrihydrite gel (f-magnetite) and (iii) biogenic magnetite derived from schwertmannite powder (s-magnetite).

Figure 3. Kinetics of 1 mM aqueous Cr(VI) reduction by synthetic magnetite, ferrihydrite derived magnetite (f-magnetite) and schwertmannite derived (s-magnetite).

Figure 4. Kinetics of aqueous Cr(VI) reduction by ferrihydrite derived magnetite (f-magnetite) and schwertmannite derived (s-magnetite) from a 1 mM solution under anaerobic conditions and a 0.5 mM solution under either anaerobic or aerobic conditions.

Figure 5. (a) XPS Fe 2*p* data and (b) XPS Cr 2*p* data obtained from (i) synthetic magnetite, (ii) ferrihydrite derived magnetite (f-magnetite) and (iii) schwertmannite derived magnetite (s-magnetite) after exposure to a 5 mM Cr(VI) solution.

Figure 6. (a) Fe $L_{2,3}$-edge XMCD spectra of (i) ferrihydrite derived magnetite (f-magnetite); (ii) f-magnetite after exposure to 5 mM Cr(VI) solution; (iii) schwertmannite derived magnetite (s-magnetite); (iv) s-magnetite after exposure to 5 mM Cr(VI) solution. Fe cation site occupancies derived from the fitting of the Fe^{2+} O_h (peak A), Fe^{3+} T_d (peak B) and Fe^{3+} O_h (peak C) using calculated spectra are given underneath each spectrum, errors are ± 0.02 cations. (b) Cr $L_{2,3}$-edge XA (i) and relative XMCD (x 5) (ii) spectra for s-magnetite (black curves) and f-magnetite (grey curves).

Figure 7. Cr(VI) concentration measured in the effluent solution from columns containing Congleton sand only (control) and biogenic magnetite derived from either ferrihydrite "gel" (f-magnetite) or synthetic schwertmannite powder (s-magnetite) as a function of time.

Figure 8. (a) Activity imaged by the gamma camera in columns containing Congleton sand only (control), a ferrihydrite derived magnetite (f-magnetite) layer and schwertmannite derived magnetite (s-magnetite) layer. The small white circular spots indicate the top and bottom of the columns. Activity seen at the foot of the image is located within the effluent containers associated with a given columns system. The bright bands in the f-magnetite and s-magnetite columns correspond to position of the magnetite layers. (b) Activity imaged within the final effluent solutions issuing from the three columns shown in figure 8(a). From left to right, the bright spots correspond to the total activity associated with columns containing Congleton sand only, ferrihydrite derived

magnetite and schwertmannite derived magnetite. All images were obtained from underneath the effluent containers.

Table 1

	Activity Detected (MBq)		
Activity Location	**control column**	**f-magnetite column**	**s-magnetite column**
Effluent	12.85	4.81	0.21
Magnetite Layer	0.00	5.60	13.79
Rest of Column	0.00	2.49	0.06
Residue in Influent	0.45	0.20	0.05
Total	13.30	13.11	14.11

Table 2

t = 38 hours	Effluent Volume (ml)	Influent Tc (MBq)	Effluent Tc (MBq)	Tc absorbed in column (%)
Control column	430	21.65	18.14	16.2
f-magnetite	372	19.92	4.40	77.9
s-magnetite	464	23.78	0.53	97.8

Figure 1

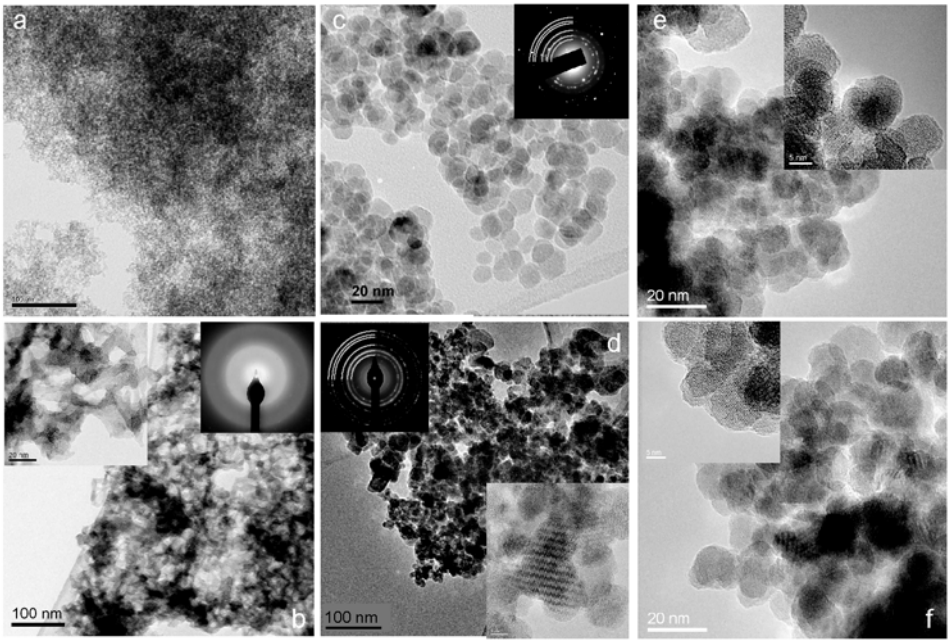

Figure 2

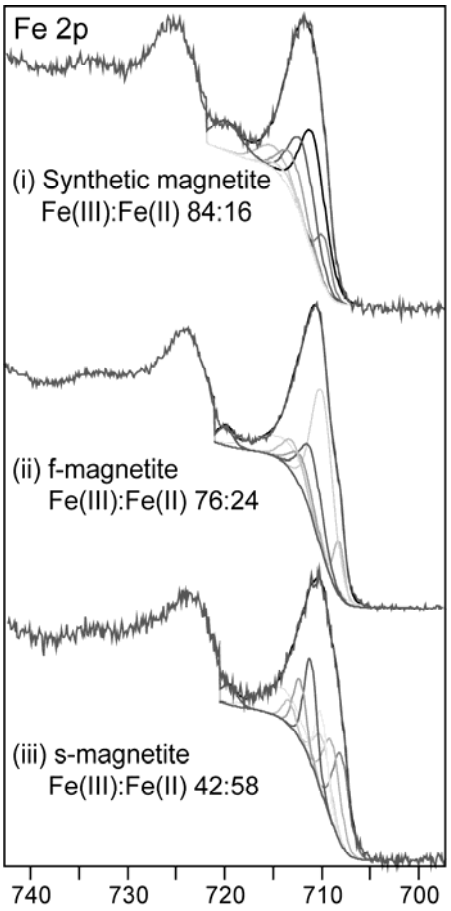
Fe 2p
(i) Synthetic magnetite
Fe(III):Fe(II) 84:16
(ii) f-magnetite
Fe(III):Fe(II) 76:24
(iii) s-magnetite
Fe(III):Fe(II) 42:58
740
730
720
710
700

Figure 3

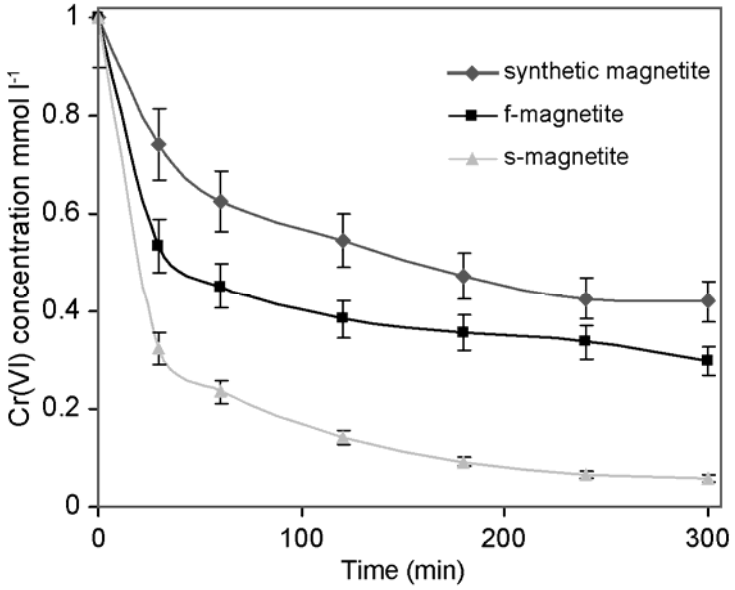
synthetic magnetite
f-magnetite
s-magnetite
Cr(VI) concentration mmol l-1
Time (min)
0
0.2
0.4
0.6
0.8
1
0
100
200
300

Figure 4

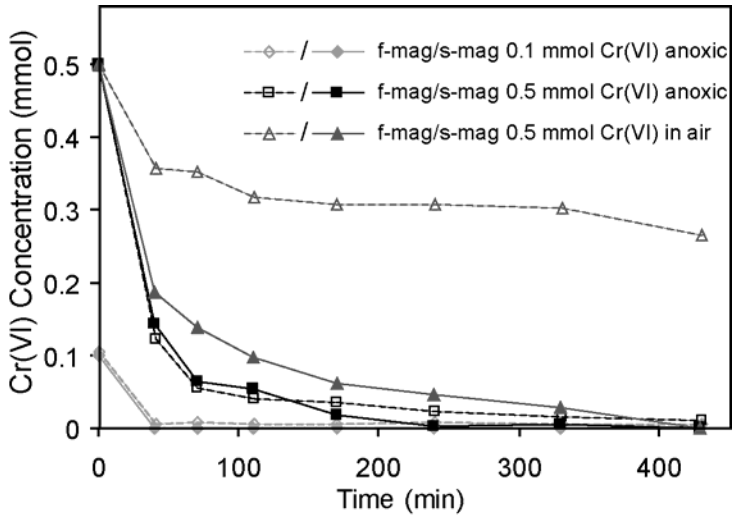
f-mag/s-mag 0.1 mmol Cr(VI) anoxic
f-mag/s-mag 0.5 mmol Cr(VI) anoxic
f-mag/s-mag 0.5 mmol Cr(VI) in air
Cr(VI) Concentration (mmol)
0
0.1
0.2
0.3
0.4
0.5
0
100
200
300
400
Time (min)

Figure 5

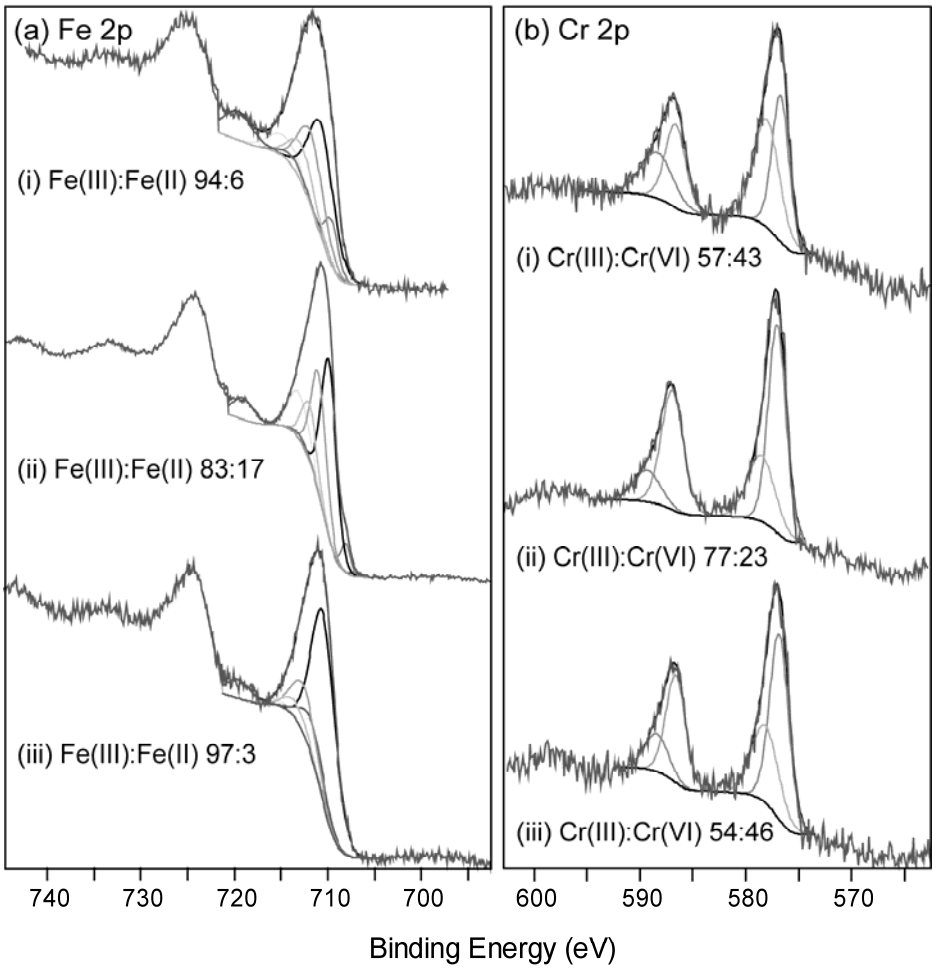
(a) Fe 2p
(i) Fe(III):Fe(II) 94:6
(ii) Fe(III):Fe(II) 83:17
(iii) Fe(III):Fe(II) 97:3
(b) Cr 2p
(i) Cr(III):Cr(VI) 57:43
(ii) Cr(III):Cr(VI) 77:23
(iii) Cr(III):Cr(VI) 54:46
740
730
720
710
700
600
590
580
570
Binding Energy (eV)

Figure 6

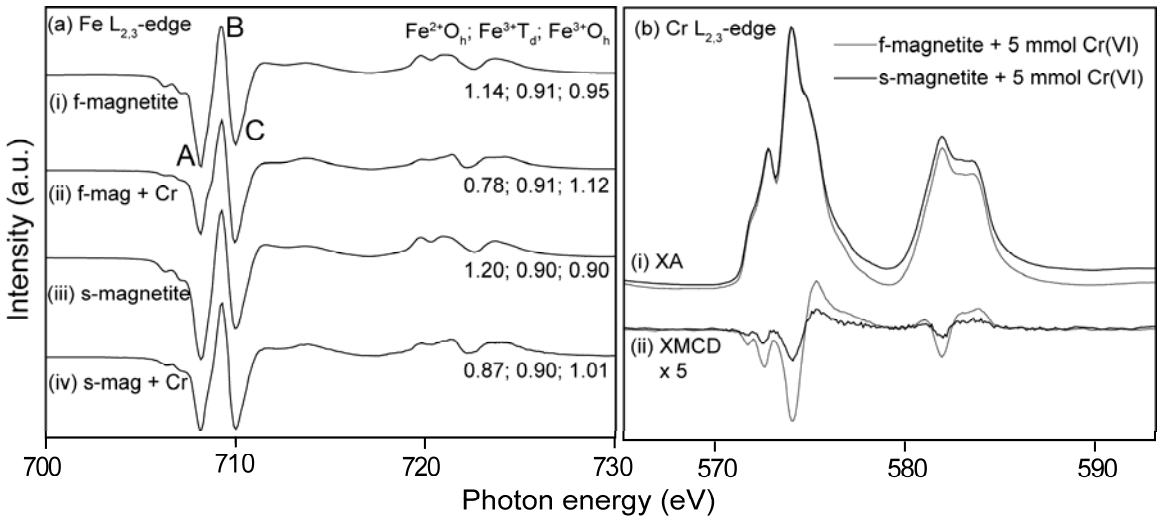
(a) Fe L2,3-edge
B
Fe2+Oh; Fe3+Td; Fe3+Oh
(i) f-magnetite
1.14; 0.91; 0.95
A
C
(ii) f-mag + Cr
0.78; 0.91; 1.12
(iii) s-magnetite
1.20; 0.90; 0.90
(iv) s-mag + Cr
0.87; 0.90; 1.01
Intensity (a.u.)
700
710
720
730
(b) Cr L2,3-edge
f-magnetite + 5 mmol Cr(VI)
s-magnetite + 5 mmol Cr(VI)
(i) XA
(ii) XMCD
x 5
570
580
590
Photon energy (eV)

Figure 7

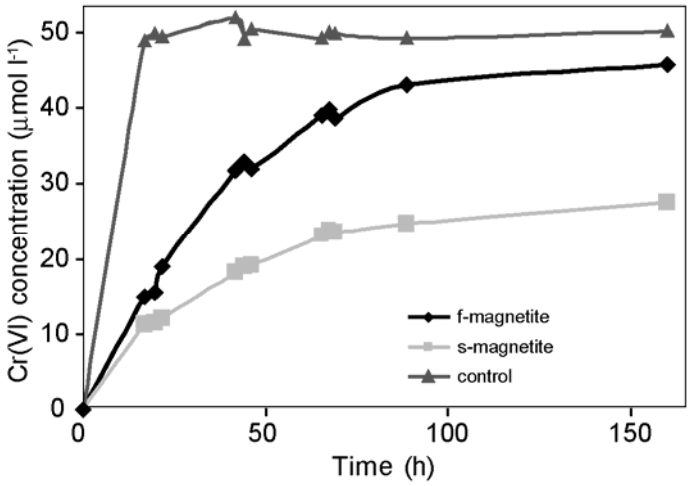
Cr(VI) concentration (µmol l-1)
0
10
20
30
40
50
0
50
100
150
Time (h)
f-magnetite
s-magnetite
control

Figure 8

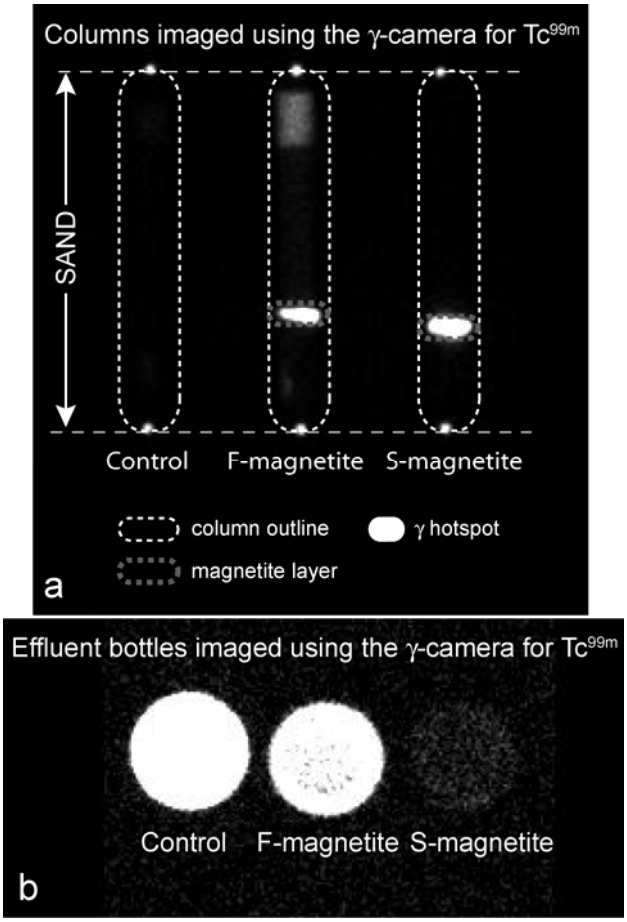
Columns imaged using the γ-camera for Tc99m
SAND
Control
F-magnetite
S-magnetite
column outline
γ hotspot
magnetite layer
a
Effluent bottles imaged using the γ-camera for Tc99m
Control
F-magnetite
S-magnetite
b